

Supplementary information for

Phase transition with in-situ exsolution nanoparticles in reduced $\text{Pr}_{0.5}\text{Ba}_{0.5}\text{Fe}_{0.8}\text{Ni}_{0.2}\text{O}_{3-\delta}$ electrode for symmetric solid oxide cells

Yunfeng Tian^{a, b}, Caichen Yang^c, Yuhao Wang^a, Min Xu^d, Yihan Ling^b, Jian Pu^c, Francesco Ciucci^{a,}

e, f, g, h*, John T.S. Irvine^d, Bo Chi^{c*}

a. Department of Mechanical and Aerospace Engineering, The Hong Kong University of Science and Technology,

Clear Water Bay, Hong Kong SAR, China.

b. School of Materials Science and Physics, China University of Mining and Technology, Xuzhou 221116, China.

c. Center for Fuel Cell Innovation, School of Materials Science and Engineering, Huazhong University of Science and Technology, Wuhan 430074, China.

d. School of Chemistry, University of St Andrews, St Andrews, Fife, KY16 9ST Scotland, UK.

*e. Department of Chemical and Biological Engineering, The Hong Kong University of Science and Technology,
Clear Water Bay, Hong Kong SAR, China*

f. HKUST Shenzhen-Hong Kong Collaborative Innovation Research Institute, Shenzhen, China.

g. HKUST Energy Institute, The Hong Kong University of Science and Technology, Hong Kong SAR, China.

h. Guangzhou HKUST Fok Ying Tung Research Institute, Nansha, Guangzhou 511458, China.

*Corresponding authors

E-mail: francesco.ciucci@ust.hk (Francesco Ciucci)

chibo@hust.edu.cn (Bo Chi)

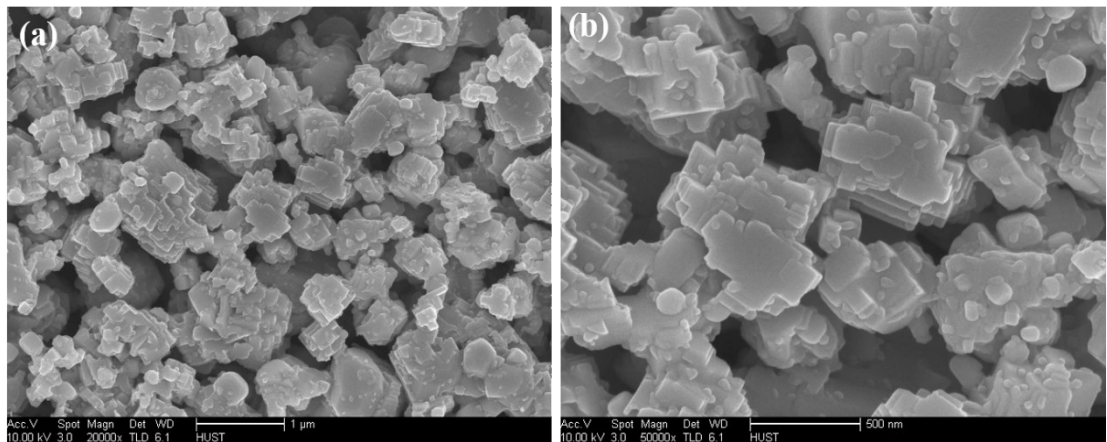


Figure S1. Micro-scale diagram of PBFN electrode after reduction.

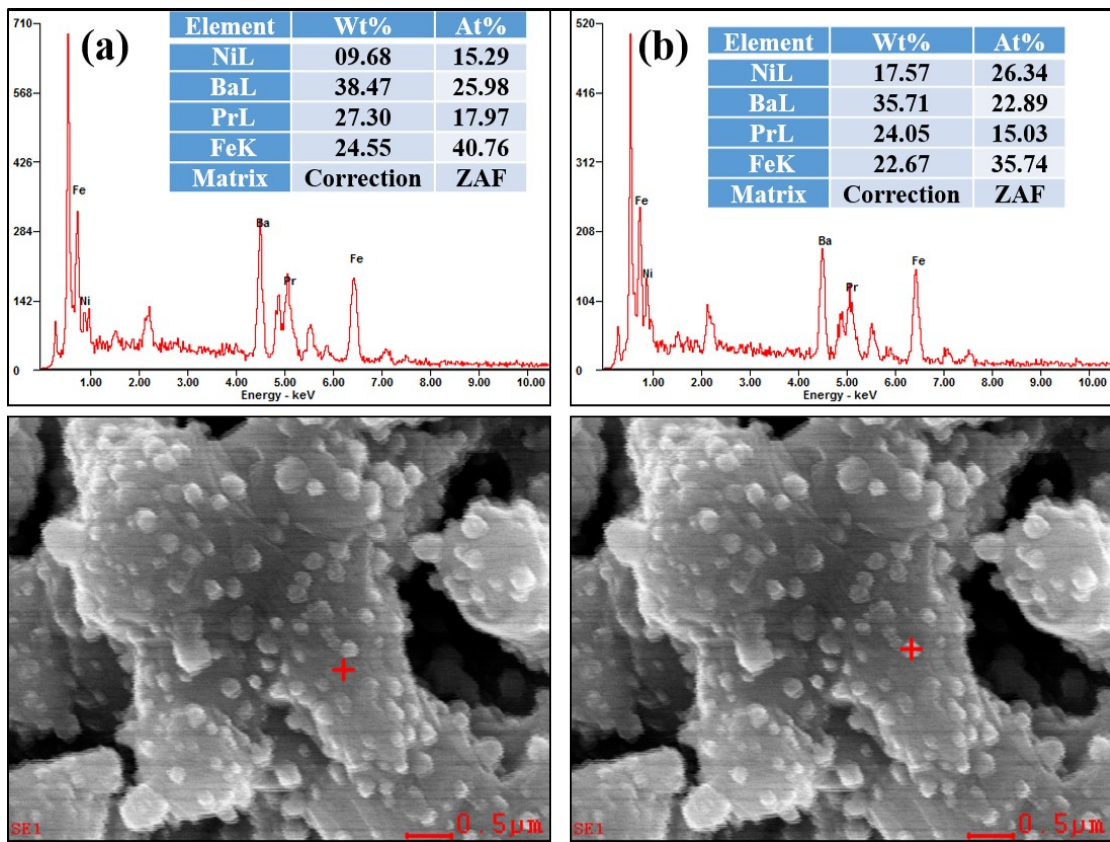


Figure S2. Microstructure of reduced PBFN electrode and the EDS analysis of the matrix (a) and exsolved nanoparticles (b).

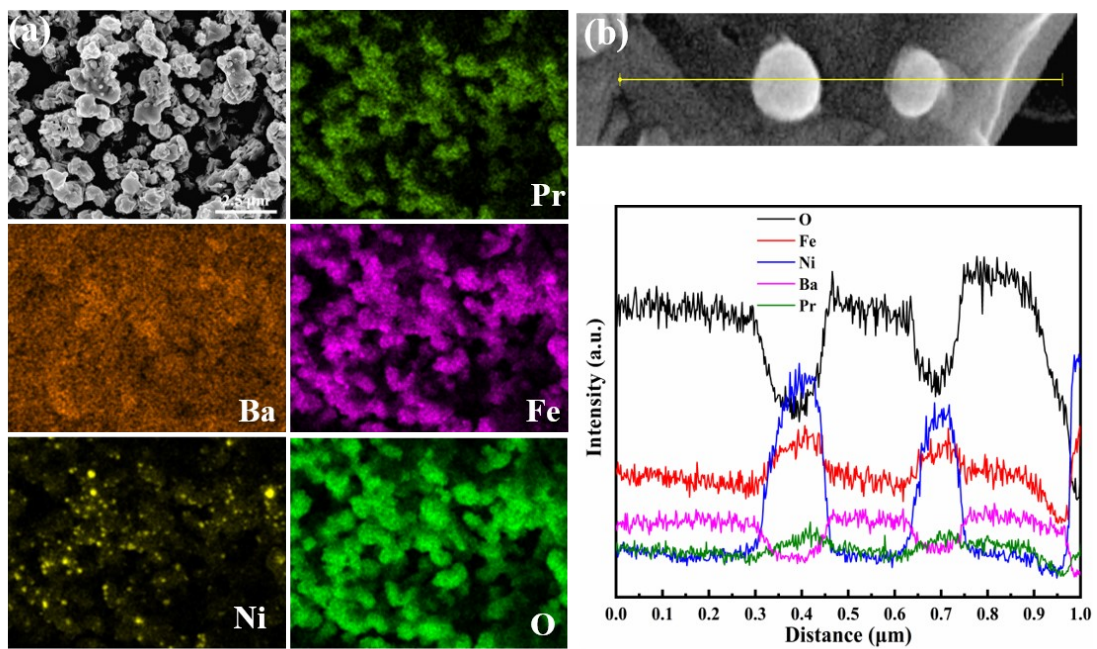


Figure S3. (a) EDS mapping of R-PBFN and (b) line scan of R-PBFN.

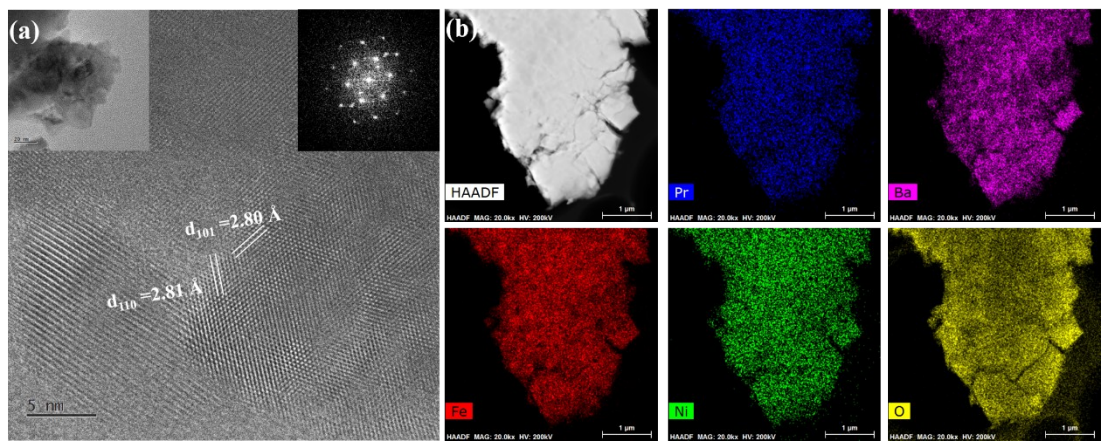


Figure S4. (a) HRTEM of PBFN, and (b) EDS map of PBFN.

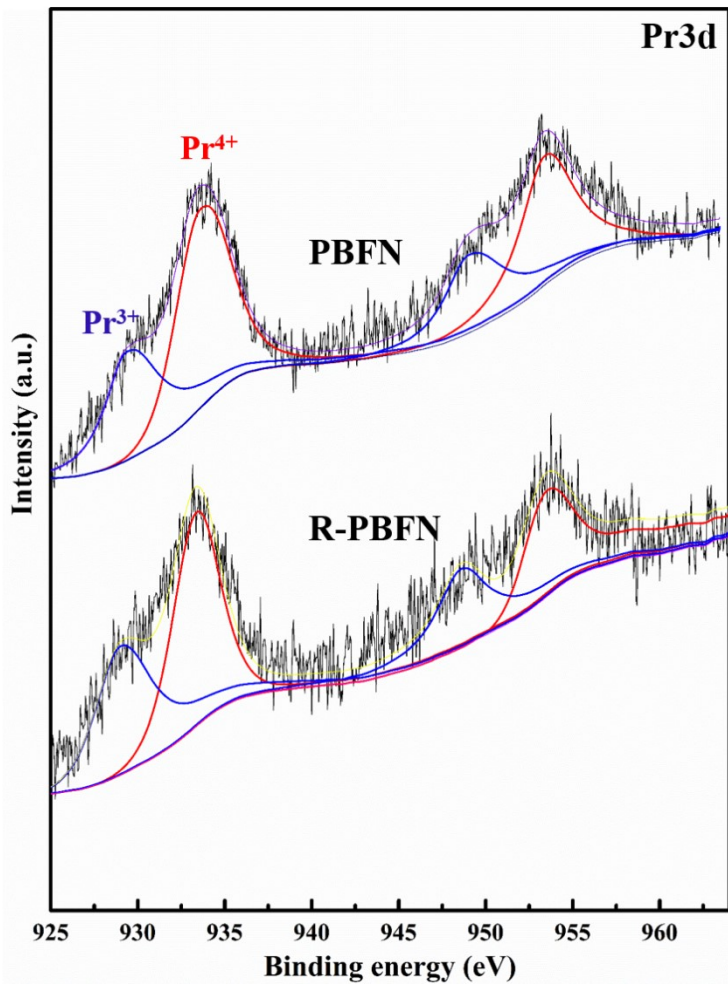


Figure S5. XPS spectra of Pr 3d.

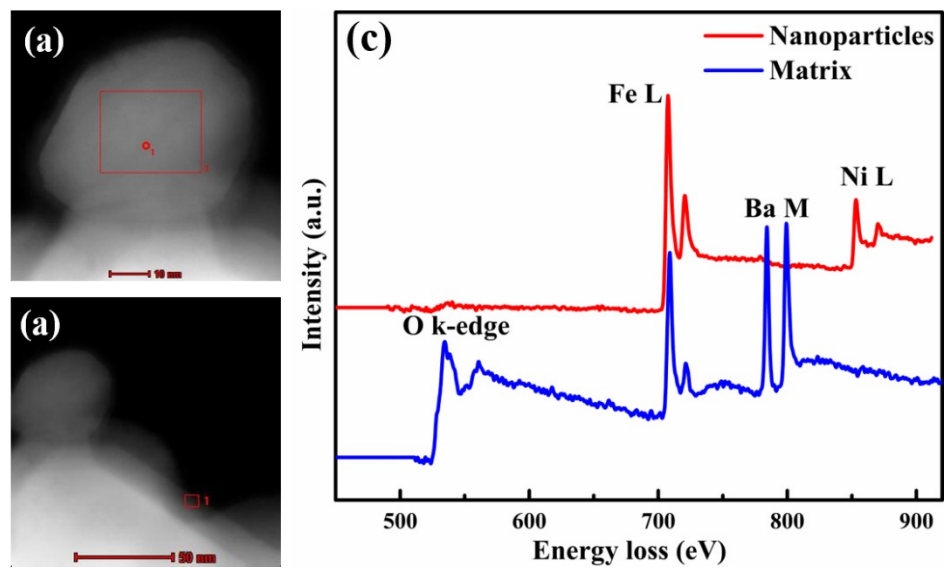


Figure S6. TEM images of R-PBFN, (a) nanoparticles, (b) matrix and corresponding EELS profiles (c).

Table S1. Electrochemical performance for symmetrical electrodes under H₂ fuel conditions in SOFC mode.

Electrode	Electrolyte	Thickness (μm)	Temperature (°C)	MPD (mW/cm ²)	R _p @OCV (Ω·cm ²)	R _p @air	R _p @H ₂	Ref
La _{0.8} Sr _{0.2} Sc _{0.2} Mn _{0.8} O ₃	SSZ	300	900	310		0.3		[1]
LaSr ₂ Fe ₂ CrO ₉	LSGM	500	800	264	0.454	0.24	0.36	[2]
La _{0.3} Sr _{0.7} Fe _{0.7} Cr _{0.3} O ₃	LSGM	500	800	300		0.1	0.4	[3]
La _{0.7} Ca _{0.3} CrO ₃	YSZ	350	850	92.1	2.17	0.15		[4]
Pr _{0.7} Ca _{0.3} Cr _{1-y} Mn _y O ₃	YSZ	370	950	250			1.5	[5]
La ₄ Sr ₈ Ti _{12-x} Fe _x O _{38-δ}	YSZ	1000	900	70			0.2	[6]
PrBaMn ₂ O _{5+δ}	YSZ	300	800	245	0.3	0.02		[7]
La _{0.6} Sr _{1.4} MnO _{4+δ}	SDC	300	800	294		0.46	0.19	[8]
La _{0.7} Ca _{0.3} Cr _{0.8} Ni _{0.2} O _{3-δ}	LSGM	400	800	254			0.08	[9]
Sm _{0.95} Ce _{0.05} FeO ₃	YSZ	700	800	130		0.15		[10]
La _{0.6} Ca _{0.4} Fe _{0.8} Ni _{0.2} O ₃	SDC	280	800	140		0.15		[11]
La _{0.8} Sr _{0.2} Fe _{0.8} Cu _{0.2} O ₃	LSGM	300	800	203	0.6		0.24	[12]
Sm _{0.9} Sr _{0.1} Fe _{0.9} Ru _{0.1} O _{3-δ}	SDC	600	800	119.69		0.3	0.93	[13]
La _{0.8} Sr _{1.2} Fe _{0.9} Co _{0.1} O ₄	LSGM	300	800	237		0.21		[14]
R-Pr_{0.5}Ba_{0.5}Fe_{0.8}Ni_{0.2}O₃	YSZ	300	800	300	0.256	0.108	0.101	This work

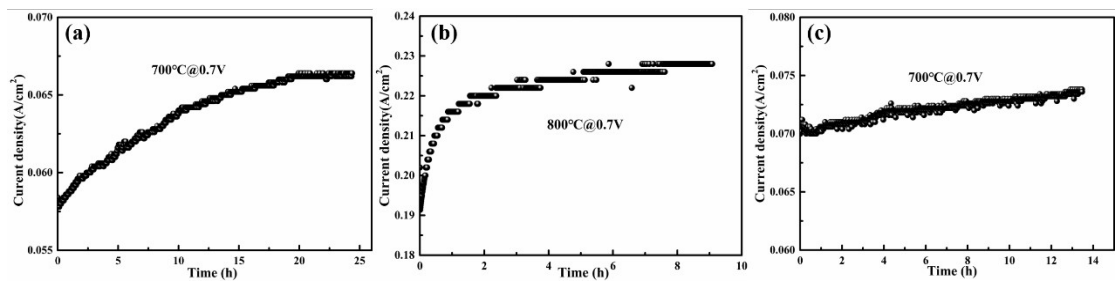


Figure S7. The short stability test in SOFC mode, first at $700^\circ\text{C}@0.7\text{V}$ (a), then increasing to 800°C (b) and decreasing to 700°C (c).

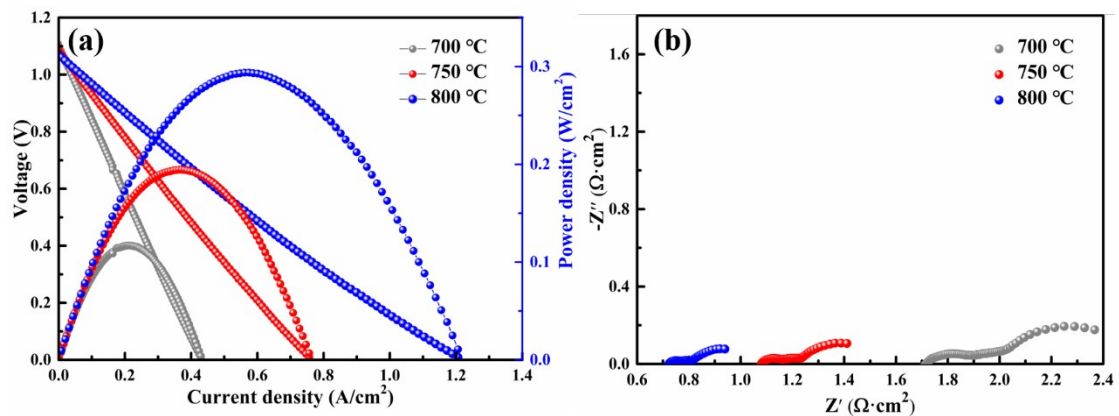


Figure S8. Symmetrical cell performance in wet hydrogen at various temperatures with R-PBFN electrode (a) I-V-P plot and EIS curves (b).

Table S2. Electrochemical performance for different electrodes for CO₂ electrolysis in SOEC mode.

Cathode	YSZ	Anode	Test	Current density (A/cm ²)	R _p (Ω·cm ²)	Ref	
	Thickness		conditions				
La _{0.75} Sr _{0.25} Cr _{0.5} Mn _{0.5} O _{3-δ}	2mm	La _{0.75} Sr _{0.25} Cr _{0.5} Mn _{0.5} O _{3-δ}	800@CO ₂	<u>0.18@2.0V</u>	<u>2.0@2V</u>	[15]	
La _{0.3} Sr _{0.7} Fe _{0.7} Cr _{0.3} O _{3-δ}	300μm	La _{0.3} Sr _{0.7} Fe _{0.7} Cr _{0.3} O _{3-δ}	800@CO ₂ :CO 90:10	<u>0.28@1.5V</u>	<u>1.33@OCV</u>	[16]	
La _{0.3} Sr _{0.7} Fe _{0.7} Ti _{0.3} O _{3-δ}	300μm	La _{0.3} Sr _{0.7} Fe _{0.7} Ti _{0.3} O _{3-δ}	800@CO ₂	<u>0.521@2.0V</u>	<u>0.08@2V</u>	[17]	
La _{0.6} Sr _{0.4} Fe _{0.9} Mn _{0.1} O _{3-δ} -GDC	200μm	La _{0.6} Sr _{0.4} Fe _{0.9} Mn _{0.1} O _{3-δ} -GDC	800@CO ₂	<u>0.521@2.0V</u>		[18]	
Exsolved	Ni	500μm	La _{0.8} Sr _{0.2} MnO _{3-δ}	800@CO ₂	<u>1.11@2.0V</u>	<u>0.51@1.6V</u>	[19]
(La _{0.2} Sr _{0.8}) _{0.95} Ti _{0.9} Mn _{0.1} Ni _{0.05} O _{3-δ}							
La _{0.7} Sr _{0.2} Ce _{0.1} Cr _{0.5} Fe _{0.5} O _{3-δ}	300μm	(La _{0.6} Sr _{0.4}) _{0.95} Co _{0.2} Fe _{0.8} O _{3-δ}	850@CO ₂ :CO 70:30	<u>0.31@2.0V</u>	<u>0.459@2V</u>	[20]	
La _{0.5} Sr _{0.5} Fe _{0.95} V _{0.05} O _{3-δ}	500μm	La _{0.8} Sr _{0.2} MnO _{3-δ}	800@CO ₂	<u>0.62@1.6V</u>	<u>0.44@1.6V</u>	[21]	
R-Pr _{0.5} Ba _{0.5} Fe _{0.8} Ni _{0.2} O _{3-δ}	300μm	Pr _{0.5} Ba _{0.5} Fe _{0.8} Ni _{0.2} O _{3-δ}	800@CO ₂	0.864@2.0V	0.88@1.4V	This Work	

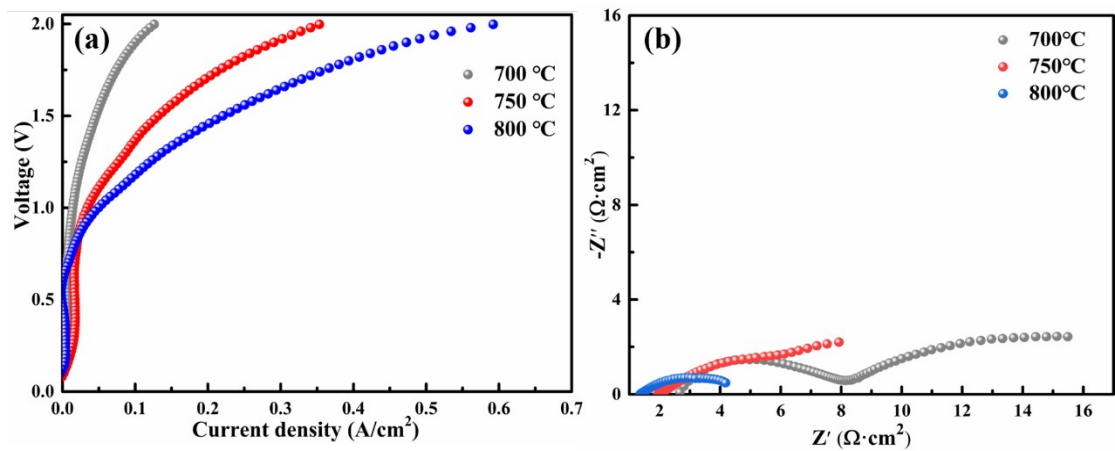


Figure S9. I-V curves (a) and EIS (b) of the PBFN based SSOC for pure CO_2 electrolysis at different temperatures.

REFERENCES

1. Y. Zheng; C. Zhang; R. Ran; R. Cai; Z. Shao; D. Farrusseng, *Acta Mater* **2009**, *57* (4), 1165-1175.
2. Q. Zhou; C. Yuan; D. Han; T. Luo; J. Li; Z. Zhan, *Electrochim. Acta* **2014**, *133*, 453-458.
3. M. Chen; S. Paulson; V. Thangadurai; V. Birss, *J. Power Sources* **2013**, *236*, 68-79.
4. B. Lin; S. Wang; X. Liu; G. Meng, *J Alloy Compd* **2010**, *490* (1-2), 214-222.
5. A. El-Himri; D. Marrero-López; J. C. Ruiz-Morales; J. Peña-Martínez; P. Núñez, *J. Power Sources* **2009**, *188* (1), 230-237.
6. J. Canales-Vázquez; J. C. Ruiz-Morales; D. Marrero-López; J. Peña-Martínez; P. Núñez; P. Gómez-Romero, *J. Power Sources* **2007**, *171* (2), 552-557.
7. Y. Gu; Y. Zhang; Y. Zheng; H. Chen; L. Ge; L. Guo, *Appl Catal B: Environ* **2019**, *257*, 117868.
8. J. Shen; G. Yang; Z. Zhang; W. Zhou; W. Wang; Z. Shao, *J. Mater. Chem. A* **2016**, *4* (27), 10641-10649.
9. M. K. Rath; K.-T. Lee, *Ceram Inter* **2015**, *41* (9), 10878-10890.
10. W. Fan; Z. Sun; J. Wang; J. Zhou; K. Wu; Y. Cheng, *J. Power Sources* **2016**, *312*, 223-233.
11. X. Ding; H. Liu; Z. Gao; G. Hua; L. Wang; L. Ding; G. Yuan, *Int. J. Hydrogen Energy* **2017**, *42* (39), 24968-24977.
12. F. Zurlo; I. Natali Sora; V. Felice; I. Luisetto; C. D'Ottavi; S. Licoccia; E. Di Bartolomeo, *Acta Mater* **2016**, *112*, 77-83.
13. W. Fan; Z. Sun; J. Zhou; K. Wu; Y. Cheng, *J. Power Sources* **2017**, *348*, 94-106.
14. J. Zhou; T.-H. Shin; C. Ni; G. Chen; K. Wu; Y. Cheng; J. T. S. Irvine, *Chem. Mater* **2016**, *28* (9), 2981-2993.
15. S. Xu; S. Li; W. Yao; D. Dong; K. Xie, *J. Power Sources* **2013**, *230*, 115-121.
16. P. Addo; B. Molero-Sánchez; M. Chen; S. Paulson; V. Birss, *Fuel Cells* **2015**, *15* (5), 689-696.
17. Z. Cao; B. Wei; J. Miao; Z. Wang; Z. Lü; W. Li; Y. Zhang; X. Huang; X. Zhu; Q. Feng, *Electrochim Commun* **2016**, *69*, 80-83.
18. X. Peng; Y. Tian; Y. Liu; W. Wang; L. Jia; J. Pu; B. Chi; J. Li, *J CO₂ Utili* **2020**, *36*, 18-24.
19. L. Ye; M. Zhang; P. Huang; G. Guo; M. Hong; C. Li; J. T. Irvine; K. Xie, *Nat. Commun.* **2017**, *8*, 14785..
20. Y.-Q. Zhang; J.-H. Li; Y.-F. Sun; B. Hua; J.-L. Luo, *ACS Appl. Mater Inter* **2016**, *8* (10), 6457-6463.
21. Y. Zhou; Z. Zhou; Y. Song; X. Zhang; F. Guan; H. Lv; Q. Liu; S. Miao; G. Wang; X. Bao, *Nano energy* **2018**, *50*, 43-51.